JOURNAL OF AIRCRAFT
Vol. 46, No. 3, May–June 2009

Drag Characteristics for Optimally Span-Loaded Planar, Wingletted, and C Wings

Joram G. Verstraeten* and Ronald Slingerland†
Delft University of Technology, 2629 HS Delft, The Netherlands

DOI: 10.2514/1.39426

This paper focuses on the drag characteristics of optimally span-loaded planar, wingletted, and C wings. The span load is optimized resulting in minimum induced or total drag. The wing-root bending moment is kept constant for all analyzed wings to ascertain that different wings have comparable weight. The optimum span loadings for the different types of wing are calculated using a fast and simple numerical method. The wings are analyzed in the Trefftz plane, infinitely far behind the wing. Lagrange multipliers are used to calculate the optimum span loading resulting in minimum induced or total drag, with the wing-root bending moment and/or the lift coefficient as constraint. The induced drag can be calculated using the optimum span loading. The profile drag is assumed to be a function of the local lift coefficient. The results indicate that the C wing does not have real aerodynamic performance advantages compared to a wingletted wing. For wings with span and/or aspect ratio constraints, a winglet offers a drag reduction relative to a planar wing.

Nomenclature

A_{ij}	=	geometric influence function
AR	=	aspect ratio
b	=	wing span, m
C_D	=	total drag coefficient
C_{D_i}	=	induced drag coefficient
C_L	=	lift coefficient
C_M	=	wing–root bending moment coefficient
c	=	chord, m
$\bar{c}$	=	mean geometric chord, m
c_{d_0}, c_{d_2}	=	profile drag coefficients
c_{d_p}	=	local profile drag coefficient
c_n	=	local normal force coefficient
J	=	objective function
L	=	lift, N
l	=	surface length or height, m
M, N	=	number of horseshoe vortices
M_b	=	wing–root bending moment, N
q_∞	=	dynamic pressure, N/m^2
S	=	wing area, m^2
s	=	nondimensional semiwidth of a vortex pair
V	=	flow velocity, m/s
V_n	=	normal velocity, m/s
v	=	velocity component in the y plane, m/s
w	=	velocity component in the z plane, downwash, m/s
x, y, z	=	aircraft coordinate system, m
y_{cp}	=	aircraft spanwise center of pressure, m
Γ	=	circulation, m^2/s
γ	=	span loading $c_n c/C_L \bar{c}$
$\delta_{\text{C wing}}$	=	nondimensional horizontal winglet length $\frac{l_{\text{C wing}}}{b/2}$
δ_{ij}	=	Kronecker delta
δ_{tip}	=	nondimensional wing-tip extension $\frac{l_{\text{tip}}}{b/2}$
δ_{winglet}	=	nondimensional winglet height $\frac{l_{\text{winglet}}}{b/2}$
η	=	nondimensional wing semispan
θ	=	rotation angle in y, z planes, rad
λ	=	Lagrangian multiplier

Subscripts

i, j	=	number designating a vortex pair that models a particular lifting element

Presented as Paper 0161 at the 46th AIAA Aerospace Sciences Meeting and Exhibit, Reno, Nevada, 7–10 January 2008; received 27 June 2008; revision received 11 December 2008; accepted for publication 11 December 2008.

*Former Student, Faculty of Aerospace Engineering, Department Design, Integration and Operation of Aircraft and Rotorcraft, Kluyverweg 1; currently Research and Development Engineer, National Aerospace Laboratory Air Transport Safety Institute (NLR-ATSI), Anthony Fokkerweg 2, 1059 CM, Amsterdam, the Netherlands. Member AIAA.

†Former Assistant Professor, Faculty of Aerospace Engineering Department Design, Integration and Operation of Aircraft and Rotorcraft, Kluyverweg 1. Former Member AIAA (Deceased).

Introduction

ONE of the reasons it takes energy to fly from one point to another is the presence of drag. The drag of a subsonic transport aircraft during cruise consists mainly of profile drag and induced drag. This paper focuses on the reduction of induced drag. Induced drag is the drag due to the creation of lift. Reducing the induced drag reduces fuel use, gas emissions, and noise emissions. One successful innovation in aircraft aerodynamic design of the last decades is the winglet. Its purpose is the reduction of induced drag. A frontal view of both a planar and wingletted wing is given in Figs. 1a and 1b. The wing semispan $\frac{b}{2}$ is indicated in the figure, as well the nondimensional winglet height δ_{winglet} and length $\delta_{\text{C wing}}$. $\delta = 1$ equals the wing semispan. Inspired by the winglet, the C wing has both horizontal and vertical winglets. A frontal view of a C wing is given in Fig. 1c.

Induced drag accounts for about 30–40% of the total drag of typical transport aircraft at cruise conditions [1,2]. At low speed, high-lift coefficient conditions, the induced drag constitutes most of the total drag. Reducing the induced drag improves low speed performance and increases the maximum possible takeoff weight, leading to, as Kroo [1] said, "an increase in range several times that associated with the simple cruise lift-to-drag ratio improvement." Therefore, reducing the induced drag is a very rewarding goal in aircraft design.

The first studies into reducing induced drag by using nonplanar wings were done by, among others, Frederick W. Lanchester [3]. He indicated that vertical surfaces located at the wing tips could significantly reduce the three-dimensional effects of airflow and thereby reduce the induced drag. Lanchester patented the endplate concept in 1897 [3]. Hemke showed that a drag reduction at higher lift coefficients was possible when using endplates [4]. Despite promising results for higher lift conditions the endplates proved to be no success. Near cruise conditions these configurations exhibited

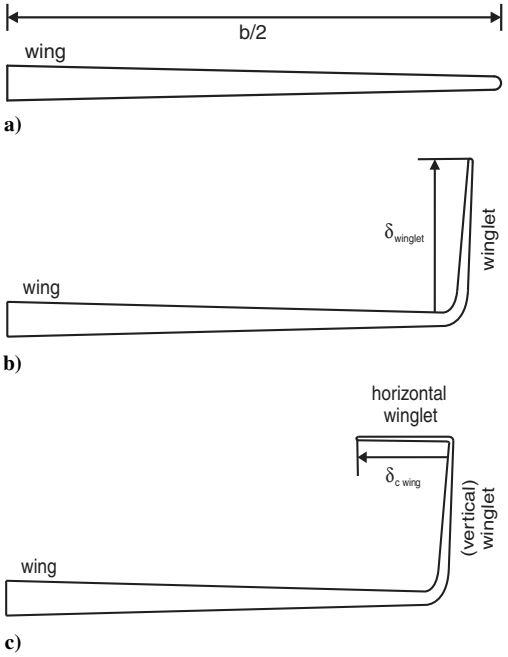

Fig. 1 Frontal view of a) planar, b) wingletted, and c) C wings.

large areas of local flow separation, resulting in large viscous drag increments, which eliminated the benefits to induced drag [3].

In the 1970s, Whitcomb of NASA's Langley Research Center realized that a vertical surface at the wing tip needs to produce significant side forces to be effective; therefore the vertical surface needs to be designed according to the well-established principles for designing efficient wings. To accentuate this need, the surfaces were named winglets [5]. Wind-tunnel and flight tests were done to determine the desired configuration of the winglets. The basic aim in the development of winglets was to provide a higher drag reduction than could be achieved with wing-tip extensions that have wing-root bending moments (WRBM) equal to those produced by winglets. The wind-tunnel tests done by Whitcomb for a representative first-generation, narrow-body jet transport wing showed an improvement in lift-to-drag ratio of roughly 9% for the design Mach number of 0.78 and near design lift coefficient, more than twice as large as achieved with a wing-tip extension resulting in the same wing-root bending moment [5]. Wind-tunnel tests on a representative second-generation wing also showed a reduction in induced drag at design condition [6].

During the same time NASA did a parametric study of the relative advantages of both winglets and wing-tip extensions [7]. This study also concluded that at an identical level of a wing–root bending moment, a winglet provides a greater induced efficiency increment than a tip extension does. A computational study by NASA showed a more relative advantage of winglets [8]. The configurations studied, one planar wing and two with winglets, converge to about the same minimum induced drag if span is increased and the integrated or wing-root bending moment kept constant. The study showed that if there are span constraints, winglets are more effective than planar wings.

Eppler [9] studied the lift due to the velocities induced by the lifting vortices on themselves, which is only present at nonplanar wings. This induced lift results in a better performance for winglets with dihedral, winglets up, than for winglets with anhedral, winglets down. This effect is only significant at higher lift coefficients. At a lift coefficient of 0.5 the difference between a winglet up or down will be very small. This study concludes that if profile drag is taken into account, the winglets will actually increase the total drag in cruise condition compared to a planar wing.

The results of the study by Eppler prompted more research into the differences between winglets with dihedral and anhedral. One study concluded that wing tips with 10 deg anhedral produce a *larger* reduction in induced drag than the same amount of dihedral [10]. A study from 2006 tested wings in a wind tunnel with a much larger variation in dihedral of the wing tip, from almost vertically down to almost vertically up. The results again showed a larger induced drag reduction compared to the baseline planar wing for wings with winglets down [11]. Ning and Kroo concluded in a 2008 study that the beneficial effect of winglets compared to tip extensions depends on the ratio of the maneuver lift coefficient to the cruise lift coefficient. For higher ratios winglets are slightly better than tip extensions [12].

A wing fitted with winglets is one of many possible nonplanar wing concepts. Kroo determined the span efficiency factors for inviscid flow for a range of these concepts with fixed height and span [1]. The C wing has a slightly larger span efficiency factor than the wingletted wing. In a study by Gage et al. a genetic algorithm was used to find a nonplanar wing with a maximum span and height, designed to minimize drag with fixed lift [13]. The algorithm eventually forms a C wing. If profile drag is included, the optimum design is a wingletted wing, however. A 2008 paper explored the topological design of nonplanar lifting surface configurations. The optimal configuration for an aerostructural optimization with sweep and taper is a C wing. Adding parasitic drag and compressibility in the analysis reduces the aerostructural optimal solution to a raked planar configuration with a winglet [14]. Ning and Kroo concluded that C wings have slightly lower drag, especially with span constraints, compared with planar wings and wings with winglets when positive pitching moments are required about the aerodynamic center [12].

McMasters et al. have studied the benefits of a C wing for a very large subsonic transport airplane [15,16]. Using a C-wing configuration, the span can be reduced without incurring a significant induced drag penalty. In the study the horizontal winglets are also used as stabilizers and as primary pitch control. This not only reduces the addition of a wetted area but also potentially provides more stability for a given area as the surfaces are not affected by the aft fuselage field and are less affected by the wing downwash. It is concluded that the sum of a number of small C-wing virtues may add up to a significant reason to pursue further development and testing [15].

The first test done by NASA with wingletted wings offered promising results. The winglet proved a success and is now fitted on aircraft ranging from sailplanes to business jets and large commercial aircraft. There is still no consensus, however, regarding the optimal design of winglets, as indicated by several studies with different conclusions mentioned above and by differences in the design of the winglets that are actually used on aircraft. It is also not clear if there is a justification for winglets as opposed to span extensions for aircraft that are not explicitly limited in span. Other nonplanar concepts such as the C wing are capable of reducing induced drag even further. The question is if the total drag of a wing will reduce using such a concept.

The numerical method used in this study to analyze wings is simple and fast. It models the wing in the Trefftz plane infinitely far behind the wing, making it possible to study many different wing configurations and get a global idea how they perform relative to each other. This way C wings with many different dimensions can be compared to winglets of different height. Furthermore, the wingletted wings can be compared to planar wings of varying span. It should be noted that the method used in this paper calculates theoretical optimum loadings resulting in minimum induced or total drag. The calculated loading must be obtained by using the right amount of aerodynamic and geometric twist. Because of the complexity of a wing, this loading can probably only be approximated in real life. Furthermore, the results are not valid for retrofitted winglets because the twist of the wing is fixed.

Although the results may not be as precise as obtained with, for example, computational fluid dynamics (CFD), it is possible to take the first steps into finding an optimal configuration, especially optimal winglet height and optimal C-wing dimensions. The optimal configuration aimed for in this paper is the configuration resulting in minimum total drag for a wing with a given lift and wing-root bending moment. If that configuration is known, CFD or other more

sophisticated tools can still be used to further optimize the chosen configuration.

Analysis

Physical Analysis of Nonplanar Wings

The basic physical effect of winglets and C wings is the diffusion of the vortex flow just downstream of the wing [6]. The mechanism by which the drag reduction due to a winglet is accomplished is twofold. A properly designed winglet creates a sideforce F, which is inclined forward due to an inward deflection of the airflow V, as seen in Fig. 2a. This deflection is caused by the flow component v_w due to the pressure difference between the lower and upper surfaces of the wing at the wing tip. The resulting thrust component T_{wl} reduces the induced drag. As seen in Fig. 2b the winglet itself also creates an induced drag component $D_{i_{wl}}$ due to the sidewash v_{wl} created by the winglet. For an optimally loaded wing with vertical winglets this induced drag exactly cancels out the thrust component according to Munk's third theorem. Munk's third theorem states that the induced drag is minimum when the following relation is satisfied [17]:

$$V_n = w \cos\theta \tag{1}$$

The theorem implies that the induced drag will be minimum when the induced velocity normal to the lifting element V_n at each point is equal to the downwash w times the cosine of the angle of inclination θ of the lifting element at that point. For a vertical winglet (90 deg inclination) this implies that the induced normal velocity at the winglet is zero, and hence the drag component $D_{i_{wl}}$ will cancel the thrust component T_{wl} out. Optimally loaded vertical winglets do, however, reduce induced drag due to a second mechanism of drag reduction.

The second mechanism by which the induced drag is reduced is a decrease in downwash of the flow approaching the wing due to the winglet. Compared to a planar wing of the same span and total lift, the spanwise lift distribution of a wingletted wing is different, which will be shown in more detail later. Relative to a planar wing, the spanwise vorticity is distributed over a larger line, that is, wing and winglet; thus for the same total lift the average downwash is decreased.

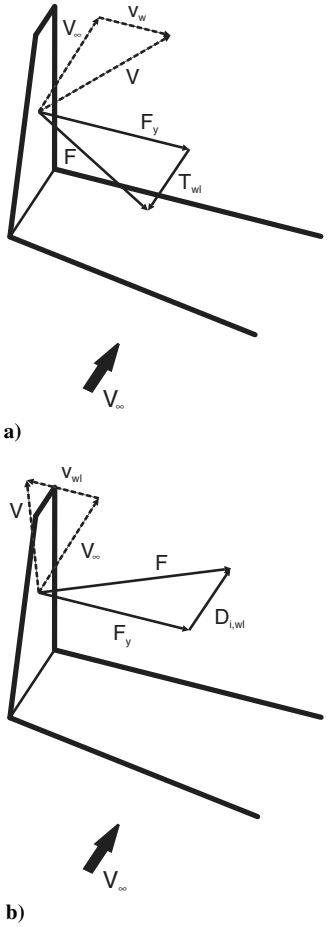

Fig. 2 Influence of a) wing on winglet and b) of the winglet on itself.

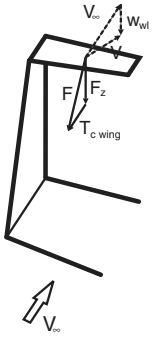

Fig. 3 Influence of winglet on horizontal winglet of a C wing.

The above is also valid for the C wing. Additionally, the horizontal surface of the C wing acts as a winglet for the vertical winglet. This implies that the load on the additional horizontal surface of the C wing needs to be orientated downward. This load is tilted forward under the influence of the flow component w_{wl} caused by the pressure difference at the vertical winglet tip, creating a thrust component $T_{\text{C wing}}$, see Fig. 3.

Numerical Method to Calculate Optimum Span Loading

This study makes use of a numerical method to calculate the optimum span loading which results in minimum induced drag for arbitrary nonplanar aircraft [17]. The optimization method used is the sequential quadratic programming method [18,19]. The aircraft lifting surfaces are represented by a system of rectangular horseshoe vortices. Using this vortex representation and Munk's three theorems, the Biot–Savart law, and the Kutta–Joukowski theorem, the induced drag for a given loading or the optimum loading for minimum induced drag can be calculated. The Kutta–Joukowski theorem gives the relation between circulation and span–load distribution. The theorem is given by

$$\frac{2\Gamma}{V_\infty \bar{c}} = \frac{c_n c}{\bar{c}} \tag{2}$$

This study concentrates on finding the optimum loading for several wing configurations.

Munk's first theorem allows all forces of the wing to be concentrated in the Y, Z plane, as indicated by the dotted line over the wing in Fig. 4. Munk's second theorem allows the computations to be done in the Trefftz plane at downstream infinity, rather than in the real plane which reduces the number of parameters used and simplifies the calculations. According to the second theorem the normal velocity calculated in the Trefftz plane at a control point

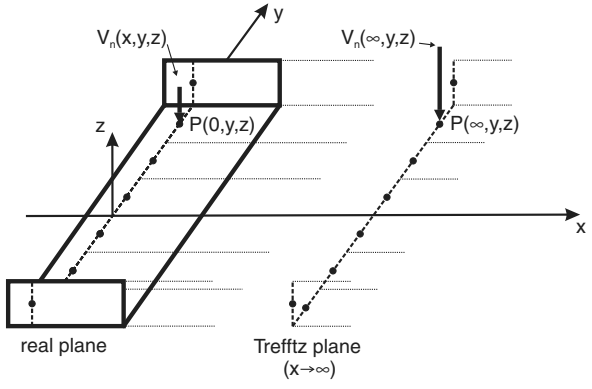

Fig. 4 Illustration of Munk's first and second theorem [17].

$P(\infty, y, z)$ is twice the actual value of the normal velocity in the corresponding control point $P(0, y, z)$ in the real plane.

In the real plane the aircraft lifting surfaces are represented by a system of horseshoe vortices. This is schematized in Fig. 4. The induced velocities in the Trefftz plane at a control point $P(\infty, y_i, z_i)$ due to a horseshoe vortex located in the real plane at point $P(x_j, y_j, z_j)$ can be derived from the Biot–Savart law. The induced velocities are functions of the circulation and wing geometry. With the Kutta–Joukowski theorem the circulation can be written in terms of span loading ($c_n c/\bar{c}$). Because the induced drag coefficient C_{D_i} is a function of the induced velocities, the induced drag coefficient can be obtained in terms of span loading and wing geometry. The lift coefficient C_L can also be written as a function of span loading and wing geometry [17]

$$C_{D_i} = \sum_{i=1}^{N} \sum_{j=1}^{N} \frac{(c_n c)_i}{\bar{c}} \frac{(c_n c)_j}{\bar{c}} s_i A_{ij} \tag{3}$$

$$C_L = 2 \sum_{j=1}^{N} \frac{(c_n c)_j}{\bar{c}} s_j \cos\theta_j \tag{4}$$

s, A, and θ are functions of the wing geometry of the aircraft. The span loading $c_n c/\bar{c}$ is the parameter that is optimized for minimum drag. c_n is the section load coefficient normal to the projection of the aircraft lifting surfaces in the Trefftz plane parallel to the YZ plane. When using the Trefftz plane it is assumed that the wake extends infinitely far downstream and trails back from the wing in the freestream direction. Therefore c_n equals the local lift coefficient c_l for a horizontal wing segment.

Optimum Span Loading Resulting in Minimum Induced Drag

To find the optimum span loading resulting in minimum induced drag, Lagrange multipliers are used [20]. An objective function J is formulated containing the function that needs to be optimized and the constraints. The most basic objective function optimizes for minimum induced drag with the lift coefficient as a constraint. The objective function in such a case is

$$J = C_{D_i} + \lambda (C_L - C_{L_{\text{inp}}}) \tag{5}$$

C_{D_i} and C_L follow from Eqs. (3) and (4). $C_{L_{\text{inp}}}$ is the desired lift coefficient, and λ is the Lagrange multiplier. The condition for minimum induced drag can be expressed by the following equation:

$$\begin{bmatrix} \frac{\partial J}{\partial \gamma_i} \\ \frac{\partial J}{\partial \lambda} \end{bmatrix} = [0] \quad \text{where } \gamma_i = \frac{(c_n c)_i}{\bar{c}} \tag{6}$$

Solving these differentiations yields a system of equations. This system can be solved to obtain a vector containing the optimum loading and as a final entry the Lagrange multiplier

$$\begin{bmatrix} \frac{(c_n c)_i}{\bar{c}} \\ \vdots \\ \lambda \end{bmatrix} = \begin{bmatrix} A_{ij} s_i + & s_i \cos\theta_i \\ A_{ij}^T s_j & \vdots \\ s_j \cos\theta_j \cdots & 0 \end{bmatrix}^{-1} \begin{bmatrix} 0 \\ \vdots \\ \frac{1}{2} C_{L_{\text{inp}}} \end{bmatrix} \tag{7}$$

The multiplier λ is only a byproduct of this method and can be disregarded, ending up with the optimum span loading that results in minimum induced drag for a certain lift coefficient.

Wing-Root Bending Moment Constraint

The wing-root bending moment is a good indicator of wing weight. By keeping the wing-root bending moment constant, it is assumed that wings of comparable weight are found and no iteration on lift is required. Heyson et al. [7] showed that there is almost a linear relationship between wing weight and the wing-root bending moment; wing weight only increases slightly more rapidly than the wing-root bending moment. The wing-root bending moment was also used as an indicator of wing weight in the first NASA studies about winglets (e.g., [5,6]). Furthermore, Klein and Viswanathan noted that "for the high-aspect ratio wings with comparatively small sweep of transport aircraft it seems to be the root-bending moment of the lift which to a large extent determines the required structural weight at cruise" [21]. The wing-root bending moment M_b is equal to the lift L times the spanwise center-of-pressure location relative to the wing root y_{cp}

$$M_b = L y_{\text{cp}} \tag{8}$$

The lift is a function of lift coefficient, dynamic pressure q_∞, and wing area S

$$L = C_L q_\infty S \tag{9}$$

Both lift coefficient and wing area are input variables, so different wings with equal input create the same amount of lift at a certain dynamic pressure or speed. The center-of-pressure location is a function of the wing-root bending moment coefficient C_M [17]

$$y_{\text{cp}} = \frac{2bC_M}{C_L} \tag{10}$$

Because the wing-root bending moment coefficient is also a function of span loading and wing geometry, it can be used as a constraint in the model, thereby keeping the spanwise center-of-pressure location constant. The wing-root bending moment coefficient can be expressed as [17]

$$C_M = \frac{1}{2} \sum_{j=1}^{N} \frac{(c_n c)_j}{\bar{c}} s \left(\frac{2y_j}{b} \cos\theta_j + \frac{2z_j}{b} \sin\theta_j \right) \tag{11}$$

With this constraint, the lift coefficient constraint, and the wing area as input it is assured that the analyzed wings have the same wing-root bending moment, and hence comparable weight. With two different multipliers λ_{C_L} and λ_{C_M}, and a moment coefficient input $C_{M_{\text{inp}}}$, the new objective function becomes

$$J = C_{D_i} + \lambda_{C_L} (C_L - C_{L_{\text{inp}}}) + \lambda_{C_M} (C_M - C_{M_{\text{inp}}}) \tag{12}$$

The condition for minimum induced drag can be expressed by

$$\begin{bmatrix} \frac{\partial J}{\partial \gamma_j} \\ \frac{\partial J}{\partial \lambda_{C_L}} \\ \frac{\partial J}{\partial \lambda_{C_M}} \end{bmatrix} = [0] \qquad \gamma_j = \frac{(c_n c)_j}{\bar{c}} \tag{13}$$

Solving these differentiations yields a system of equations. This system can be solved to obtain a vector containing the optimum span loading resulting in minimum induced drag with the lift and wing-root bending moment coefficient as constraints. The final two entries are the Lagrange multipliers, which can be disregarded,

$$\begin{bmatrix} \frac{(c_n c)_j}{\bar{c}} \\ \vdots \\ \vdots \\ \lambda_{C_L} \\ \\ \lambda_{C_M} \end{bmatrix} = \begin{bmatrix} A_{ij} s + & 2s\cos\theta_j & s\frac{y_j}{b}\cos\theta_j + \\ A_{ij}^T s & \vdots & s\frac{z_j}{b}\sin\theta_j \\ & \vdots & \vdots \\ s\cos\theta_i \cdots & 0 & 0 \\ s\frac{2y_i}{b}\cos\theta_i + & 0 & 0 \\ s\frac{2z_i}{b}\sin\theta_i \cdots & & \end{bmatrix}^{-1} \begin{bmatrix} 0 \\ \vdots \\ \vdots \\ \frac{1}{2} C_{L_{\text{inp}}} \\ \\ 2C_{M_{\text{inp}}} \end{bmatrix} \tag{14}$$

Optimum Span Loading Resulting in Minimum Total Drag

The wings can also be optimized for minimum total drag. The total drag is the induced drag plus the profile drag. It is assumed that the profile drag can be written as a function of the local lift coefficient [20] and therefore also as a function of span loading

$$c_{d_p} = c_{d_0} + c_{d_2} c_n^2 \tag{15}$$

$$c_{d_p} = c_{d_0} + c_{d_2}\left(\frac{c_n c}{\bar{c}}\right)^2\left(\frac{\bar{c}}{c}\right)^2 \tag{16}$$

where c_{d_p} is the local profile drag coefficient, and c_{d_0} and c_{d_2} are constants. Equation (16) can be integrated over the wing span and added to Eq. (3). Now a new objective function containing the total drag coefficient can be used to optimize for minimum total drag (for simplicity in explaining the method, only the lift coefficient constraint is used)

$$J = C_D + \lambda_{C_L}(C_L - C_{L_{\text{inp}}}) \tag{17}$$

Differentiating this objective function yields a system of equations. Solving this system one obtains a vector containing the optimum span loading resulting in minimum total drag

$$\begin{bmatrix} \frac{(c_n c)_j}{\bar{c}} \\ \vdots \\ \lambda_{C_L} \end{bmatrix} = \begin{bmatrix} A_{ij}s + & 2s\cos\theta_j \\ A_{ij}^T s + D_p & \vdots \\ s\cos\theta_i \cdots & 0 \end{bmatrix}^{-1} \begin{bmatrix} 0 \\ \vdots \\ \frac{1}{2}C_{L_{\text{inp}}} \end{bmatrix} \tag{18}$$

where $D_p = 4\delta_{ij} s c_{d_2} \dfrac{\bar{c}}{c_j}$

Results

Method Verification

To verify the method, the results obtained for a planar wing using the current method are compared to the results obtained for such a wing by Prandtl [22]. Figure 5 shows the span–load distribution (here divided by C_L, $c_n c/C_L\bar{c}$, and denoted in the graphs with γ) of a planar wing optimized for minimum induced drag; the result is an elliptical load distribution. The method used here only has a very small error with a magnitude that depends on the number of horseshoe vortices used per semispan. In Fig. 6 the number of vortices is plotted against the span efficiency factor e. The span efficiency factor of an elliptically loaded planar wing is 1. For the right balance between speed and accuracy most of the calculations are done using 200 vortices per semispan. The span efficiency factor calculated for an optimally loaded planar wing using 200 vortices per semispan is 1.0025, an error of only 0.25%. The additional surfaces of nonplanar wings use an equivalent number of vortices, for example, a winglet with a height of 10% of the semispan uses 20 vortices.

Optimum Span Loadings

The span loadings resulting in minimum induced drag for wingletted and C wings are plotted in Fig. 7a, together with the elliptical load. The lift coefficient is 0.5. The span loadings of the additional surfaces of the nonplanar wings are plotted as if they are attached to the wing in the horizontal plane. The actual direction of the span loadings on the different surfaces is given in Fig. 8. Both nonplanar wings make use of additional surfaces of 20% semispan at a 90 deg angle. The wing with winglet shows a large increase in load at the wing tip, compensated by a lower load at the root. The load at the wing tip of the C wing is even larger, but is compensated by the lower load at the root and by the downward load on the horizontal winglet. The span efficiency factors associated with these wings are 1.22 and 1.25, equivalent to a reduction in induced drag coefficient of

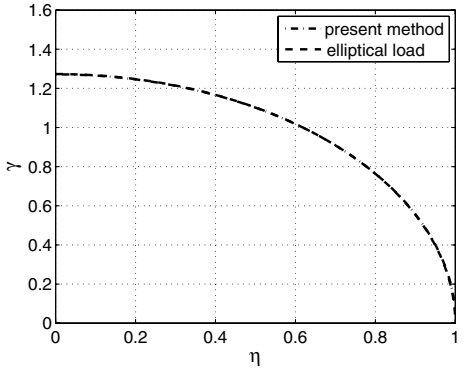

Fig. 5 Optimum span loading ($c_n c/C_L\bar{c}$), resulting in minimum induced drag for a planar wing.

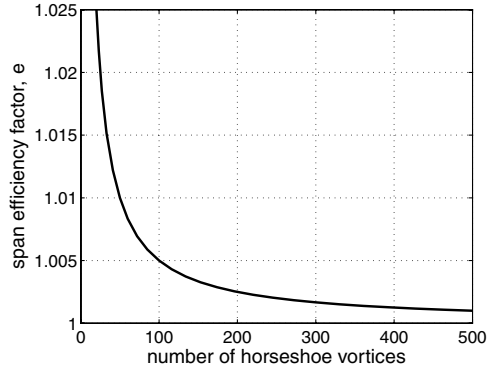

Fig. 6 Relation between number of horseshoe vortices and span efficiency factor.

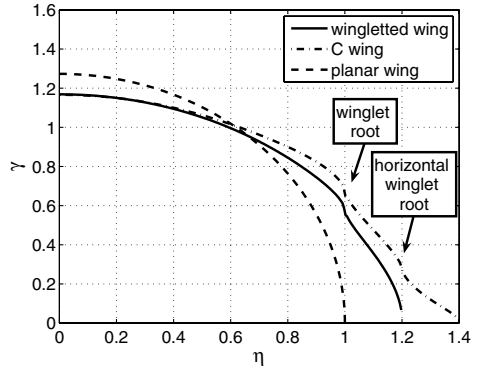

a) Lift coefficient constraint

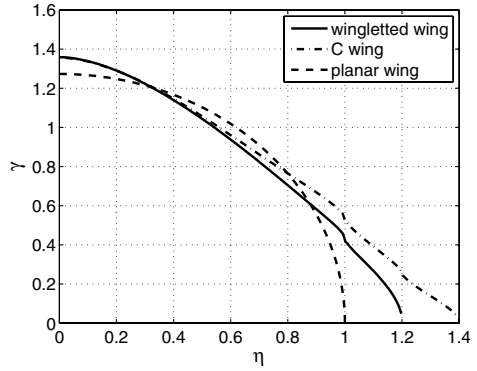

b) Lift coefficient and WRBM constraint

Fig. 7 Optimum span loading resulting in minimum induced drag for planar, wingletted, and C wings.

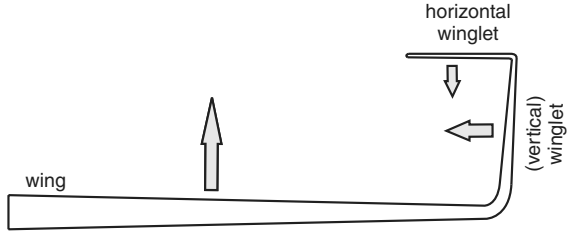

Fig. 8 Positive direction of span loadings on different wing surfaces.

18 and 20%, respectively, for wings with the same lift coefficient and aspect ratio.

Figure 7b shows the optimum loading that results in minimum induced drag for a wingletted and C wing with the WRBM constraint. The loading of the nonplanar wings *without* WRBM constraint have far more load at the tip region of the wing. Combined with the loading of the winglet, the optimum load results in a shift of the center of pressure toward the wing tip, increasing wing weight. Therefore the optimum span loadings calculated with WRBM constraint have more loading at the wing root, and less at the tip relative to the optimum span loadings calculated without WRBM constraint. This results in a wing-root bending moment equal to the planar wing, but a drop in span efficiency factor compared to the nonplanar wings analyzed without WRBM constraint. The span efficiency is still significantly higher than a planar wing, namely, 1.16 for the wingletted wing and 1.19 for the C wing, equivalent to a reduction in induced drag coefficient of 14 and 16%, respectively. The optimum loading resulting in minimum total drag is not significantly different from the loadings resulting in minimum induced drag.

Induced Drag Coefficient per Surface

The numerical method of this paper can be used to study the sources of induced drag and the mechanisms of induced drag reduction. Equation (3) can be used to calculate the induced drag components of a surface (wing, winglet, or horizontal winglet) under influence of one of the surfaces. For example, the induced drag component of the wing due to the winglet of a wingletted wing can be calculated using

$$C_{D_i\text{wing,winglet}} = \sum_{i=1}^{N} \sum_{j=N+1}^{N+M} \frac{(c_n c)_i}{\bar{c}} \frac{(c_n c)_j}{\bar{c}} s A_{ij} \tag{19}$$

where N is the number of control points on the wing, and M the number of points on the winglet. The results are given in Table 1 for four wings: a planar, a wingletted, and a C wing without WRBM constraint, and a wingletted wing with WRBM constraint. The lift coefficient is 1 to obtain more convenient induced drag numbers; a negative number indicates an induced drag decrease. The table contains some interesting results. First consider the wingletted wing without WRBM constraint. The thrust component of the winglet due to the wing is negated by the induced drag created by the winglet itself, as indicated by Munk's third theorem. The winglet of the wingletted wing with WRBM constraint does create some thrust, albeit very little. The main mechanism by which the induced drag is reduced for both wingletted wings is the influence of the winglet on the wing. The results of the C wing give good insight into the influences of the three surfaces on each other. The sum of the induced drag coefficients of the vertical winglet equals zero. The sum of the induced drag coefficients of the horizontal winglet is negative, indicating a thrust vector is created at the horizontal winglet. The influence of the wing on the horizontal winglet and vice versa is only very small in magnitude. The influence of the winglet of the C wing on the wing results in a much larger induced drag reduction than for the wingletted wing. The combination of the thrust vector and larger influence of the winglet on the wing only causes a small reduction in total induced drag relative to the wingletted wing, due to the fact that the induced drag coefficient of the wing due to the wing itself on the C wing is significantly higher than for the wingletted wing.

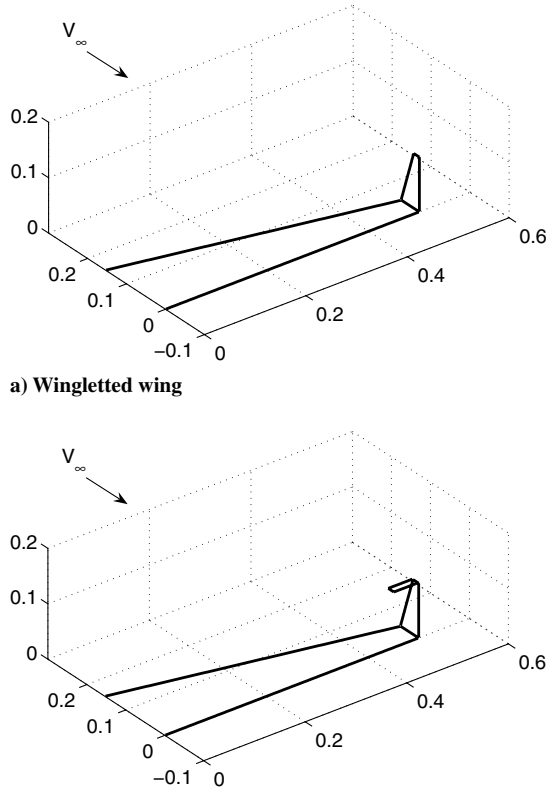

a) Wingletted wing

b) C wing

Fig. 9 Planforms of wingletted and C wings.

Drag Characteristics

Wingletted Wings

A larger winglet surface will increase span efficiency and hence decrease induced drag. However, the profile drag will increase. By incorporating the profile drag in the model an optimum winglet height can be found. The profile drag is a function of the profile drag coefficients (c_{d_0} and c_{d_2}) and the wing planform. For the profile drag coefficients and the wing planform parameters, some assumptions must be made to be used in the remainder of the paper. The planforms of a wingletted wing with an arbitrary winglet height of 20% of the semispan, and a C wing with an arbitrary winglet height of 20% and horizontal winglet length of 10% of the semispan are plotted in Fig. 9. The taper ratios of both wing and winglet are 0.3, and the taper ratio of the horizontal winglet of the C wing is 1. The aspect ratio is 10 for both wings. Both profile drag coefficients are assumed to be 0.005. The lift coefficient used is 0.5.

Table 1 Induced drag contribution per surface due to a surface; $C_L = 1$

Induced drag coefficient	Due to	Planar wing	Wingletted wing	Wingletted wing, WRBM constraint	C wing
Wing	Wing	0.0318	0.0398	0.0356	0.0454
Wing	Winglet		−0.0138	−0.0079	−0.0192
Wing	Horizontal winglet				−0.0002
Winglet	Wing		−0.0137	−0.0079	−0.0192
Winglet	Winglet		0.0137	0.0078	0.0222
Winglet	Horizontal winglet				−0.0030
Horizontal winglet	Wing				−0.0002
Horizontal winglet	Winglet				−0.0030
Horizontal winglet	Horizontal winglet				0.0025
Total		0.0318	0.0260	0.0276	0.0253

Figure 10a shows the difference in drag coefficient between a planar wing and a wing with varying winglet height. In the figure the nondimensional winglet height δ_{winglet} is relative to the wing semispan, that is, $\delta_{\text{winglet}} = 1$ indicates a winglet height equal to the wing semispan. The optimum winglet height is around 75% of the semispan resulting in a decrease in drag coefficient of 11.7%. Beyond that height the increase in profile drag outweighs the decrease in induced drag. The optimum wingletted wing has a 36% larger wing-root bending moment than the planar wing, resulting in a significantly larger weight. The winglet seems unrealistically high. This could be caused by the chosen constants of the profile drag assumption and the fact that the assumption does not take Reynolds number effects into account. Because of the smaller chord of the winglet relative to the wing, the Reynolds number will be lower, and therefore the influence of the winglet on the profile drag will be larger in reality.

By keeping the wing-root bending moment constant, a wing with and without winglet of comparable weight can be analyzed. Figure 10b shows the result. The optimal winglet height is now 28% of the semispan and the drag decrease is 5.4%. Clearly, when the wing span is constrained the winglet can offer a significant reduction in drag. The optimum winglet is still higher than any winglet currently fitted on commercial aircraft. Those winglets are designed taking into account more design constraints than minimizing total drag. Those other constraints could include structural constraints, costs, and in the case of a retrofit the specific loading of the wing. Some aircraft designed by Rutan use similarly large winglets as the optimum found in this paper. In those designs the winglet also acts as a vertical stabilizer. This does not validate the results of this paper per se, but does show that aircraft could be fitted with winglets with substantial height.

C Wings

A comparison of a wing with winglets of 28% semispan with a C wing with equal vertical winglet height and varying horizontal winglet length and equal wing-root bending moment is presented in Fig. 11. Surprisingly, no matter the length of the horizontal winglet, the C wing performs worse than the wingletted wing. In other words, an optimally loaded wingletted wing with optimum winglet height cannot be improved by adding a horizontal surface to the winglet tip. It is not certain, however, that a C wing has the same optimum vertical winglet height as a wingletted wing. Figure 12 shows the total drag reduction of a wingletted wing with varying winglet height compared to a planar wing, similar to Fig. 10b. For every winglet height it also shows the maximum possible drag reduction if a horizontal surface with an optimum length is attached to the winglet tip, creating a C wing. The optimum horizontal winglet length for a certain vertical winglet height is plotted as well. The C wing only performs slightly better for winglet heights up to about 25% of the semispan. The maximum optimum horizontal winglet length is 3.5% of the wing semispan, for winglet heights between 7 and 15%. The maximum drag reduction relative to a wingletted wing with equal vertical winglet height is only on the order of 0.1%. The C wings plotted in Fig. 12 that perform worse than the wingletted wings have an optimum horizontal winglet length equal to zero. No C wing can be found that performs better than the wingletted wing with optimum winglet height. It can be concluded from these results that it is very questionable if there is any real aerodynamic advantage to the use of C wings if total drag is considered.

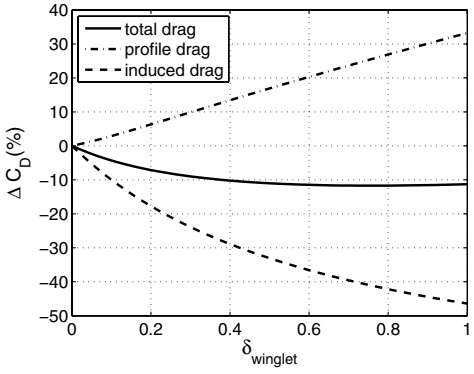

a) Equal span

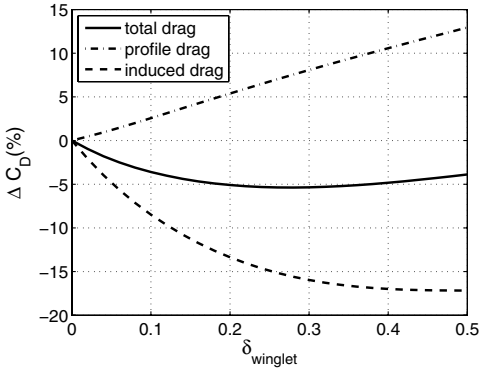

b) Equal span and wing-root bending moment

Fig. 10 Difference in drag between wingletted wings and a planar wing.

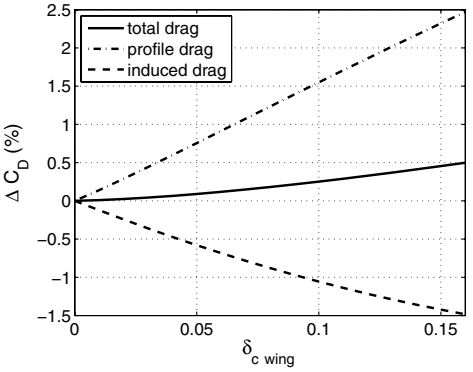

Fig. 11 Difference in drag of C wings and a wingletted wing ($\delta_{\text{winglet}} = 0.28$).

Extended Wing vs Wingletted Wing

The reduction of drag due to a winglet can also be achieved by increasing the wing span of a planar wing. For a fair comparison the wingletted and extended wings analyzed here have the same wing-root bending moment and lift as an unextended elliptically loaded planar base wing. The lift of the extended planar wing can be kept constant in two ways, assuming a constant dynamic pressure. The lift coefficient and wing area can be kept constant for both wings, or the wing area of the extended wing can be increased, and the lift coefficient decreased such that the product of both parameters, $C_L S$, is constant. In the first method the wing area is kept constant by decreasing the root and tip chord, while maintaining a taper ratio of

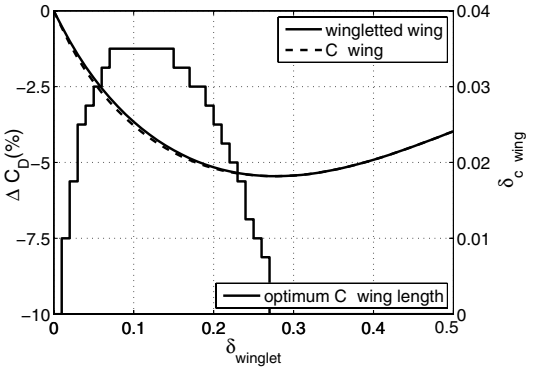

Fig. 12 Total drag reduction of wingletted wings compared to the best C-wing configurations.

0.3. In the second method the wing is extended by keeping the root chord constant and keeping the same leading-edge and trailing-edge lines. This results in an increasing wing area and a decreasing taper ratio.

First the method of keeping the wing area constant is used. In Fig. 13a the wing-tip extension and associated aspect ratio needed to achieve the same drag reduction as wingletted wings with varying winglet heights are plotted. All wings analyzed have the same wing-root bending moment and lift as the optimally loaded planar base wing with aspect ratio 10. The needed tip extensions to match the drag reduction of the wingletted wings are significantly smaller than the winglet heights. A span extension of 6.7% of the semispan is needed to achieve the same drag reduction as a wingletted wing with optimum winglet height of 28% of the wing semispan. The aspect ratios are still acceptable compared to the base value of 10. Figure 14a shows the planforms of a wingletted wing with optimal winglet height and an extended planar wing with the same wing-root bending moment, lift, and drag.

The second method gives somewhat different results. Because the wing area is altered when using the second method it is not sufficient to compare drag coefficients. Drag is equal to $C_D q_\infty S$, so for a certain dynamic pressure $C_D S$ needs to be equal for the compared wings to have equal drag. The tip extension is restricted to a maximum because of the decreasing taper ratio. As can be seen from Fig. 13b the needed wing-tip extensions to achieve the same drag as wingletted wings are larger than for the first method. The needed span extension to achieve the same drag reduction as a wingletted wing with optimum winglet height is 8.7%. The corresponding aspect ratios are about the same as for the first method, however. Figure 14b shows the planforms of both wings.

It can be concluded that for every wingletted wing an extended wing with equal performance can be found. The wing does not have to be extended significantly. The wing can be extended further to perform even better than the wingletted wing, although the increasing aspect ratio introduces other problems for transport aircraft.

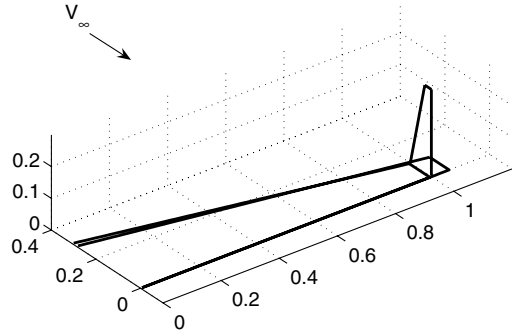

a) Constant wing area

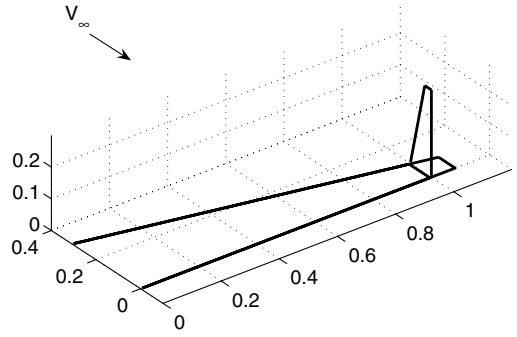

b) Constant $C_L S$

Fig. 14 Planform of a wingletted wing and an extended wing with equal drag.

Extended Wings with Winglets

Figure 15 shows the drag reduction of extended wings relative to an unextended base wing as a function of the tip extension for both methods of keeping the lift constant. With both methods a drag reduction can be obtained larger than possible with a wingletted wing

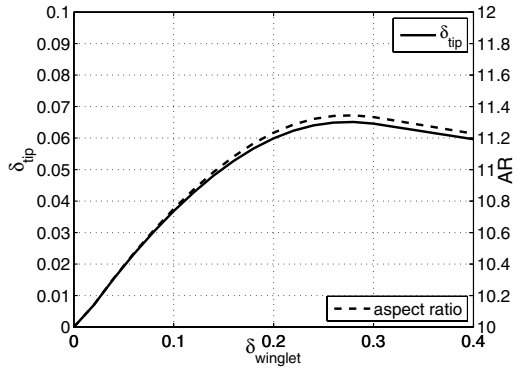

a) Constant wing area

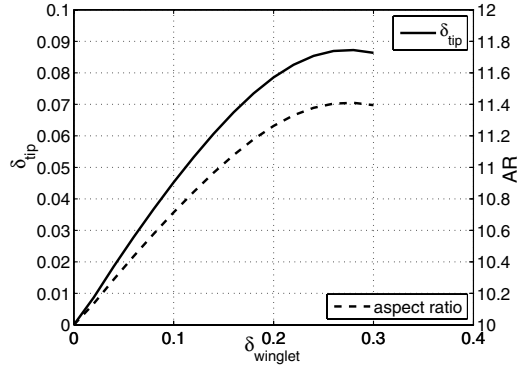

b) Constant $C_L S$

Fig. 13 δ_{tip} and AR needed for the same drag reduction as wingletted wings.

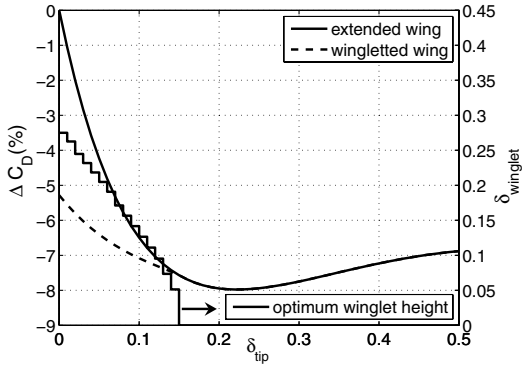

a) Constant wing area

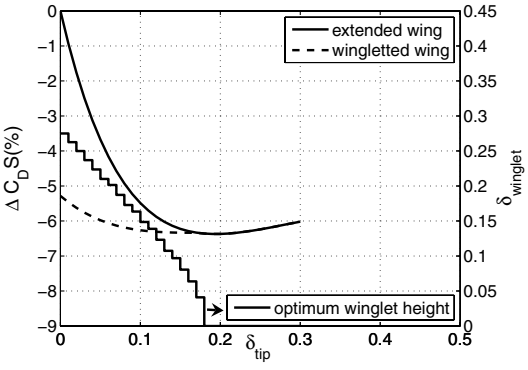

b) Constant $C_L S$

Fig. 15 Drag reduction of extended and optimum wingletted wings relative to a planar wing.

with optimum winglet height. However, an extended wing can be fitted with a winglet as well, without increasing the span. Therefore, Fig. 15 also shows the influence of a vertical winglet of optimum height on the performance of the extended wing. For every tip extension analyzed, the optimum winglet height for that particular extended wing is found and its drag performance plotted. This is done for both methods of keeping the lift constant. All wings analyzed have the same wing-root bending moment and lift as a base planar wing with aspect ratio of 10. The optimum winglet height is relative to the base wing of unit span. In other words, a winglet height of 0.20 equals 20% of the semispan of the unextended base wing.

The plots contain quite some information. First consider the method of keeping the wing area constant, Fig. 15a. Some of the previous results can be found in this plot as well. Relative to the base wing an unextended wingletted wing with 28% semispan winglet height achieves a drag reduction of a bit more than 5%, as we have seen in Fig. 10b. That performance can also be achieved by an extended wing with approximately 7% semispan extension as seen before. The plot also contains new information. Up to 15% semispan tip extension wingletted wings of equal span can be found that perform better than the extended planar wings. The best possible performance is achieved by an extended planar wing with a tip extension of around 22% of the semispan. The total reduction relative to the base wing is 8%. That performance cannot be improved by adding a winglet.

Figure 15b shows the performance of extended planar and wingletted wings for the method of keeping $C_L S$ constant. Here the reduction in $C_D S$ is compared for all wings. The drag reduction is smaller than achieved by the first method. The wingletted wing performs better up to 18% semispan tip extension. The best performance for an extended wing can also be reached by a wingletted wing with a smaller span. The best extended wing has a tip extension of almost 20% semispan and a drag reduction of 6.4%. The same reduction can be achieved with a 13% extended wingletted wing with 11% semispan winglet height. No wing performs better than the best wing from Fig. 15a.

Figure 16 shows the span loading of the extended wing with minimum drag, as found in Fig. 15a, compared to an elliptically loaded planar wing with equal lift and wing-root bending moment. The reader is reminded that the x axis is the nondimensional wing semispan. The tip extension is 22% of the semispan. The extended wing has significantly more loading at the root. The loading at the tip region is less. The loading is so small at the tip region that a winglet will not be effective and does not reduce the drag further, as is clear from Fig. 15a.

Summarizing Figs. 15a and 15b, it is clear that the best performance can be reached using an extended planar wing. A disadvantage of extending a wing without changing the wing area significantly is an increase in aspect ratio. Figure 17 shows the aspect ratio for the extended wings, with a base wing of aspect ratio 10. Clearly the aspect ratio becomes too large at some point. For the best performing wing, the 22% extended planar wing using the method of keeping the wing area constant, the aspect ratio is around 15.

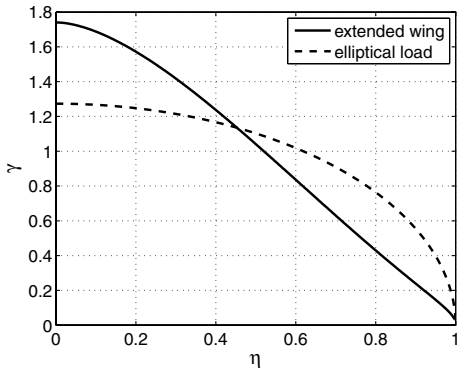

Fig. 16 Optimum span loading resulting in minimum drag for an optimally extended planar wing.

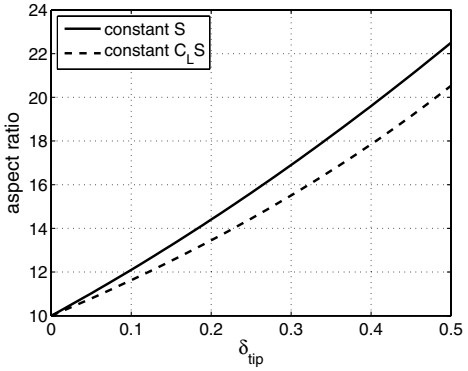

Fig. 17 Aspect ratio as a function of span extension.

For many aircraft there are constraints to the aspect ratio. For subsonic transport aircraft the aspect ratio ranges from about 6 (McDonald Douglas DC-10) to 12 (Fokker 50). The deflection along a high-aspect ratio wing tends to be much higher than for one of low-aspect ratio, resulting in higher stresses and higher risk of fatigue and flutter. Low-aspect ratio wings tend to be more naturally stable, resulting in handling advantages, especially at low speeds. Furthermore, low-aspect ratio wings have a greater useful internal volume, which can be used to house the fuel tanks, landing gear, and other systems. Span limits for airport gates also limit the aspect ratio of commercial aircraft. Because of this restriction in aspect ratio, winglets have definitive advantages over wing-tip extensions. Although the maximum drag decrease relative to a base wing can be achieved with an extended wing, the wingletted wing is capable of higher drag reductions if there are constraints to the aspect ratio. Therefore, it can be concluded that there are justifications for winglets when the span is constraint, but also justifications for winglets opposed to span extensions only, because of constraints to aspect ratio.

Conclusions

The method presented in this paper can be used to get a global idea of the performance of several planar and nonplanar wing configurations. Although the results are approximations of the actual performance of the wings, the method can be used to quickly assess how different configurations compare to each other and which trends they follow when surface sizes are altered and constraints imposed. An optimally loaded nonplanar wing produces less induced drag than an elliptically loaded planar wing. If profile drag is incorporated an optimum winglet height of a wingletted wing of 75% of the wing semispan is found. The drag is reduced by 11.7% relative to the elliptically loaded planar wing, but the wing-root bending moment is increased by 36%. A wingletted wing with the wing-root bending moment of an optimally loaded planar wing has an optimum winglet height of 28% of the semispan. The drag reduction is 5.4%. It can be concluded that winglets provide a drag reduction when the wing span is constrained.

C wings that perform marginally better than wingletted wings with the same wing-root bending moment can be found for vertical winglet heights up to 25% of the semispan. The maximum drag reduction relative to a wingletted wing with equal winglet height is only on the order of 0.1%. There is no C wing that performs better than the wingletted wing with optimal winglet height of 28% of the semispan. Therefore, it is concluded that there is no real aerodynamic performance advantage of the C wing compared to the wingletted wing.

The drag can also be reduced by increasing the wing span of a planar wing but keeping the wing-root bending moment constant. The maximum drag reduction that can be achieved by an extended wing is 8.0% for a tip extension of 22% of the semispan. The aspect ratio of such a wing is 15. The extended planar wing can also be fitted with a winglet. No extended wingletted wing achieves a higher drag reduction than the 22% extended planar wing. For smaller tip

extensions, and hence lower aspect ratios, winglets fitted on extended wings do provide an additional drag reduction relative to planar wings with the same span. It can therefore be concluded that if there are constraints to the aspect ratio, winglets can be used to reduce induced drag. Subsonic transport aircraft aspect ratios range from 6 to 12, indicating there are constraints to the aspect ratio.

The recommendations for future work on this topic fall into three categories, namely, related to the profile drag estimation, the incorporation of weight in the model, and the optimization goal. The profile drag estimation used in this paper was relatively simple. The approximation can be improved by incorporating the Reynolds number effect due to differences in chord length between the wing and the winglet. The Reynolds number of the winglet is lower than the wing, resulting in a larger influence on the profile drag.

The way weight is accounted for in the model can be improved. In the present model it is assumed the wing-root bending moment is a good indication of wing weight. A proper weight estimation should include the actual weight of the additional surfaces. This additional weight also causes a decrease in wing-root bending moment, decreasing the wing weight. This inertia relief can be incorporated in the model as well. This paper found span loadings optimized for minimum induced and total drag. The aerodynamic optimum resulting in minimum drag is not necessarily the most preferable optimum. Using the lift-to-drag ratio and the ratio of gross weight to empty weight, the span loading can be optimized for maximum range. Finally, the optimization method could include variable winglet cant, to find the optimum winglet cant angle.

References

[1] Kroo, I. M., "Drag due to Lift: Concepts for Prediction and Reduction," *Annual Review of Fluid Mechanics*, Vol. 33, Jan. 2001, pp. 587–617. doi:10.1146/annurev.fluid.33.1.587

[2] McCormick, B. W., *Aerodynamics, Aeronautics, and Flight Mechanics*, 2nd ed., Wiley, New York, 1995.

[3] Chambers, J. R., "Winglets," *Concept to Reality: Contributions of the NASA Langley Research Center to U.S. Civil Aircraft of the 1990s*, NASA SP-2003-4529, Oct. 2003, http://oea.larc.nasa.gov/PAIS/Concept2Reality/winglets.html [retrieved 7 Dec. 2008].

[4] Hemke, P. E., "Drag of Wings with End Plates," NACA No. 267, 1928.

[5] Whitcomb, R. T., "A Design Approach and Selected Wind-Tunnel Results at High Subsonic Speeds for Wing-Tip Mounted Winglets," NASA, TN D-8260, July 1976.

[6] Flechner, S. G., Jacobs, P. F., and Whitcomb, R. T., "A High Subsonic Speed Wind-Tunnel Investigation of Winglets on a Representative Second-Generation Jet Transport Wing," NASA, TN D-8264, July 1976.

[7] Heyson, H. H., Riebe, G. D., and Fulton, C. L., "Theoretical Parametric Study of the Relative Advantages of Winglets and Wing-Tip Extensions," NASA, TP-1020, Sept. 1977.

[8] Jones, R. T., and Lasinsky, T. A., "Effect of Winglets on the Induced Drag of Ideal Wing Shapes," NASA, TM-81230, Sept. 1980.

[9] Eppler, R., "Induced Drag and Winglets," *Aerospace Science and Technology*, Vol. 1, No. 1, 1997, pp. 3–15. doi:10.1016/S1270-9638(97)90019-5

[10] Gold, N., and Visser, K. D., "Aerodynamic Effects of Local Dihedral on a Raked Wingtip," AIAA Paper 2002-0831, Jan. 2002.

[11] Gerontakos, P., and Lee, T., "Effects of Winglet Dihedral on a Tip Vortex," *Journal of Aircraft*, Vol. 43, No. 1, 2006, pp. 117–124. doi:10.2514/1.14052

[12] Ning, S. A., and Kroo, I. M., "Tip Extensions, Winglets, and C-Wings: Conceptual Design and Optimization," AIAA Paper 2008-7052, Aug. 2008.

[13] Gage, P. J., Kroo, I. M., and Sobieski, I. P., "Variable-Complexity Genetic Algorithm for Topological Design," *AIAA Journal*, Vol. 33, No. 11, Nov. 1995, pp. 2212–2217. doi:10.2514/3.12969

[14] Perez, R. E., Jansen, P. W., and Martins J. R. R. A., "Aerostructural Optimization of Non-Planar Lifting Surface Configurations," AIAA Paper 2008-5967, Sept. 2008.

[15] McMasters, J. H., and Kroo, I. M., "Advanced Configuration for Very Large Transport Airplanes," *Aircraft Design*, Vol. 1, No. 4, Dec. 1998, pp. 217–242. doi:10.1016/S1369-8869(98)00018-4

[16] McMasters, J. H., Paisley, D. J., Hubert, R. J., Kroo, I. M., Bofah, K. K., Sullivan, J. P., and Drela, M., "Advanced Configurations for Very Large Subsonic Transport Airplanes," NASA, CR-198351, Oct. 1996.

[17] Blackwell, J. A., Jr., "Numerical Method to Calculate the Induced Drag or Optimum Loading for Arbitrary Non-Planar Aircraft," NASA SP-405, May 1976.

[18] Gill, P. E., Murray, W., and Wright, M. H., "Optimality Conditions," *Practical Optimization*, Academic Press, San Diego, 1981, p. 76.

[19] Nocedal, J., and Wright, S. J., "Sequential Quadratic Programming," *Numerical Optimization*, Springer–Verlag, Berlin, 1999, pp. 528–574.

[20] Kroo, I. M., "Design and Analysis of Optimally-Loaded Lifting Systems," AIAA Paper 84-2507, Oct. 1984.

[21] Klein, A., and Viswanathan, S., "Minimum Induced Drag of Wings with Given Lift and Root-Bending Moment," *Zeitschrift für Angewandte Mathematik und Physik (ZAMP)*, Vol. 24, No. 6, 1973, pp. 886–892. doi:10.1007/BF01590797

[22] Anderson, J. D., Jr., "Incompressible Flow Over Finite Wings," *Fundamentals of Aerodynamics*, 3rd ed., McGraw–Hill, New York, 2001, pp. 351–417.